A Less-Memory and High-Efficiency Autofocus Back Projection Algorithm for SAR Imaging

Kebin Hu, Xiaoling Zhang, *Member, IEEE*, Shufeng He, Hanxing Zhao, and Jun Shi, *Member, IEEE*

***Abstract*—The back projection (BP) algorithm is an accurate time-domain imaging method for synthetic aperture radar. However, the influences of wind field and turbulence on the platform make the antenna phase centers (APCs) greatly deviate from the designed linear trajectory and degrade the BP performance. Although the inertial measurement unit can be used to measure the trajectory, the measurement error still affects the image quality to some extent. The autofocus BP algorithm under the criterion of maximum image sharpness has been proposed to compensate the motion error effectively. However, this method needs to compute and store the per-pulse back-projected values for all pixels, which results in the heavy burden for memory and time and limits its practical application. This letter demonstrates an improved way to overcome these two drawbacks without loss of focusing performance. In our new method, only minority pixels are selected for autofocus to estimate the phase error, which is used to obtain the APCs by solving a system of nonlinear equations with an optimization method. This procedure is particularly suitable for the wide application of the autofocus BP. The experimental results strongly validate the efficacy and efficiency of the improved autofocus BP algorithm.**

***Index Terms*—Autofocus, back projection (BP), motion error compensation (MEC), synthetic aperture radar (SAR).**

I. Introduction

SYNTHETIC aperture radar (SAR) [1] has been deeply researched and widely applied for its all-weather and all-time capabilities. However, due to the effect of platform vibration, wind field [2], and turbulence [3], the antenna phase center (APC) of airborne SAR might greatly deviate from the ideal trajectory. This influence degrades the image quality drastically and makes the motion error compensation (MEC) [4] very important for high-precision imaging.

The back projection (BP) algorithm [5] is an accurate and potential imaging method for real-time system. The main MEC method for BP is based on the inertial measurement unit (IMU) [6]; nevertheless, the common IMU cannot satisfy the requirement for high-precision APC. To get higher image quality, the autofocus BP algorithms have been proposed. In [7], the phase gradient algorithm (PGA) [8] was introduced into the BP algorithm, and good performance is obtained. In [9], a scheme to compatibly blend a novel multiple aperture map drift (MD) algorithm [10] with fast factorized BP [11] was presented, but it can only compensate the low-order phase error just as the traditional MD algorithm. Both of the two methods imbedded the traditional autofocus methods into the BP algorithm, but this idea is not generally applicable because the corresponding Fourier relationship is not identical for different configurations.

The more advanced method is to optimize the image index that can reflect the image focus. An autofocus BP based on the minimum image entropy criterion is shown in [12], with which the area target can be focused. However, the slow convergency speed diminishes this method's application for large scene imaging. In [13], Ash proposed an effective and promising autofocus BP for small-scene and spotlight SAR (also fits for side-looking SAR as mentioned in the literature) based on the maximum image sharpness criterion. Because this method uses all the pixels, it can be referred to as "global autofocus BP (GABP)." The most valuable point of GABP is that it demonstrated a natural geometric interpretation that allows for optimal single-pulse phase corrections to be derived in closed form as the solution of a quartic polynomial. In this way, the time consumption is reduced by a large amount. However, GABP needs to compute and store the per-pulse back-projected values for all pixels, which results in heavy burden for memory and time and limits its practical application.

Based on the GABP in [13], this letter proposes an improved autofocus BP algorithm. In this method, only several pixels are involved in the autofocus to estimate the phase error, and then, the phase error is used to obtain the APC by solving the simplified systems of equations with the optimization method. As an excellent result, the computation burden and the memory requirement can be largely reduced. Since this improved method uses local pixels, it is called "local autofocus BP (LABP)" for short. The same as GABP, the imaging quality of LABP can be well guaranteed if the range error is less than several meters.

This letter is organized as follows. Section II illustrates the general principle of GABP. Section III deduces the APC estimation method with the optimization method. In Section IV, the point target simulation and the real data experiment are performed. Section V concludes this letter.

II. GABP

The geometry of monostatic SAR is sketched in Fig. 1. The blue dashed line indicates the ideal straight trajectory, while the red solid line indicates the actual curve trajectory. $\boldsymbol{p}_{i,k}$ and $r_{i,k}$ denote the kth $(k = 1, 2, \ldots, K)$ ideal platform position and range between the target and the platform, respectively. $\boldsymbol{p}_{a,k}$ and $r_{a,k}$ denote the kth actual position and range, respectively. $\boldsymbol{p}_{p,m}$ denotes the mth $(m = 1, 2, \ldots, M)$ position of the point target.

Manuscript received May 15, 2014; revised August 7, 2014, September 24, 2014, and October 20, 2014; accepted October 25, 2014. Date of publication November 20, 2014; date of current version January 6, 2015. This work was supported by the Natural Science Fund of China under Grant 61101170.

The authors are with the University of Electronic Science and Technology of China, Chengdu 610054, China (e-mail: kbhu_work@126.com).

Color versions of one or more of the figures in this paper are available online at http://ieeexplore.ieee.org.

Digital Object Identifier 10.1109/LGRS.2014.2365612

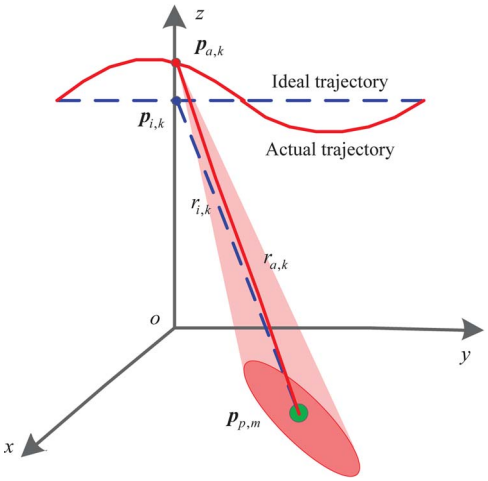

Fig. 1. SAR geometry with motion error.

BP algorithm is an accurate imaging method, but this is under the condition of known accurate APC. For monostatic SAR, the compensation term for the accurate BP is

$$\Phi = e^{j2\omega r_{a,k}/c} \tag{1}$$

where ω is the carrier frequency; c is the speed of light. If there is no IMU or other measurement sensors, $r_{i,k}$ is used instead of $r_{a,k}$ in practice, and $r_{i,k}$ can be calculated through the rough initial platform position and the constant speed. Then, the compensation error will be

$$\Delta\Phi = e^{j2\omega\Delta r_k/c} \tag{2}$$

where

$$\Delta r_k = r_{a,k} - r_{i,k}. \tag{3}$$

Although IMU has been widely used to obtain the APC, the measurement error will also result in phase error and decrease the image quality, particularly for high-resolution imaging.

In order to compensate these phase errors, the autofocus BP algorithm under the criterion of maximum image sharpness is proposed in [13], which is abbreviated to "GABP" as this autofocus method aims at optimizing the whole image space. GABP estimates the per-pulse phase error vector $\boldsymbol{\phi} = [\phi_1, \phi_2, \ldots, \phi_K]^T$ through the following unconstrained optimization prototype:

$$\hat{\boldsymbol{\phi}} = \arg\max_{\boldsymbol{\phi}\in\mathbb{R}^K} f(\boldsymbol{\phi}) \tag{4}$$

where the target function $f(\boldsymbol{\phi})$ is the sharpness of the image; $\mathbb{R}^K$ denotes the K-dimensional real space. To calculate the sharpness, all the information of the whole scene is used, which results in two major drawbacks.

First, the required memory to store the back-projected values is (in double precision)

$$M_p = 8 \times M \times K \quad \text{bytes}. \tag{5}$$

M_p dramatically increases with the scene size since the per-pulse back-projected values for all the pixels in the scene need to be stored. For example, let $M = 2000 \times 2000$ and $K = 5000$, and then, the required memory should be about 149 GB. This high memory demand is very difficult to be satisfied on usual processors. In [13], it is stated that the per-pulse back-projected values can be computed as needed without storing them. In this way, although the memory is reduced, the time consumption will greatly increase as the computation of the per-pulse back-projected values is removed into each iteration.

As for the time consumption, even if the per-pulse back-projected values of the the whole scene are computed out of the iteration, it still costs plenty of time. Moreover, too much time is spent on other operations of large intermediate matrices in each iteration.

III. Improved Autofocus BP

From the aforementioned section, we can see that the primary cause of vast storage and low efficiency of GABP is the large optimization space. Therefore, a feasible way to improve the performance of GABP is reducing the size of the optimization space. From the aspect of the BP algorithm, the accurate APC is the key factor for high-precision imaging indeed. Therefore, it is not necessary to compensate the phase error for every pixel at each slow time in each iteration if we can estimate the APC through the autofocus for less pixels. Based on this scheme, we propose an improved autofocus method to estimate the APC in this section. We only make use of several pixels to estimate the phase error vector with GABP, and then, this phase error vector is used to compute the APC according to the relationship of phase error to APC. Compared with GABP, this improved method uses much less pixels, so it can be referred to as "LABP."

Suppose that the phase error vector is $\boldsymbol{\phi}$. Then, the relationship of the slant range error $\Delta\hat{\boldsymbol{r}}$ for one pixel to the estimated phase error $\hat{\boldsymbol{\phi}}$ is

$$\Delta\hat{\boldsymbol{r}} = \frac{\lambda}{2\pi}\hat{\boldsymbol{\phi}}. \tag{6}$$

For the monostatic configuration, $\Delta\hat{\boldsymbol{r}}$ denotes the two-way range error. Then, the estimated two-way slant range is

$$\hat{\boldsymbol{r}} = \tilde{\boldsymbol{r}} - \Delta\hat{\boldsymbol{r}} \tag{7}$$

where $\tilde{\boldsymbol{r}}$ denotes the rough slant range calculated through the straight trajectory.

After we get the two-way slant range $\hat{\boldsymbol{r}}$, the relationship of $\hat{\boldsymbol{r}}$ to APC should be required to get the APC. This relationship can be gained according to the SAR geometry, which is

$$\hat{r}_{k,m} = 2\|\boldsymbol{p}_{a,k} - \boldsymbol{p}_{p,m}\|_2 \tag{8}$$

where $\hat{r}_{k,m}$ denotes the slant range between the kth APC and the mth pixel; $\|\cdot\|_2$ denotes the L2-norm.

Equation (8) for all k's and m's can be combined into a system of nonlinear equations, which contains $K \times M$ equations. Because there are K APC vectors in the three spatial coordinates, the number of unknown variables in (8) is $K \times 3$. Theoretically, only three targets are required to solve this system, i.e., $M = 3$.

Now, if the phase error $\hat{\boldsymbol{\phi}}$ is known, this equation system can be solved. In fact, $\hat{\boldsymbol{\phi}}$ can be obtained through the same principle and iterations as in GABP. Moreover, in order to reduce the

memory requirement and the computation, we select only three targets for autofocus since only three targets are needed to solve this equation system. Although less targets are used, the autofocus effect can be retained if the selected targets are relatively strong points. The reason is that the strong point plays the biggest role in the computation of sharpness and the focus of the strong point represents the quality of the whole image. This principle is identical to PGA [8].

The optimization method is selected to solve this system of nonlinear equations. One advantage of this solution is that it can accommodate a more flexible situation, in which more pixels can be used to form an overdetermined system and to get much higher precision. However, this system contains too many equations, and the convergence of the optimization method may be slow, so we separate this system to K independent subsystems, each including three equations and only solving one APC. The kth subsystem is

$$\begin{cases} \hat{r}_{k,1} = 2\|\boldsymbol{p}_{a,k} - \boldsymbol{p}_{p,1}\|_2 \\ \hat{r}_{k,2} = 2\|\boldsymbol{p}_{a,k} - \boldsymbol{p}_{p,2}\|_2 \\ \hat{r}_{k,3} = 2\|\boldsymbol{p}_{a,k} - \boldsymbol{p}_{p,3}\|_2. \end{cases} \tag{9}$$

By removing $\hat{r}_{k,m}$ to the right side, (9) can be written as

$$\begin{cases} f_1(\boldsymbol{p}_{a,k}) = 0 \\ f_2(\boldsymbol{p}_{a,k}) = 0 \\ f_3(\boldsymbol{p}_{a,k}) = 0 \end{cases} \tag{10}$$

where

$$f_m(\boldsymbol{p}_{a,k}) = 2\|\boldsymbol{p}_{a,k} - \boldsymbol{p}_{p,m}\|_2 - \hat{r}_{k,m}, \qquad m = 1, 2, 3. \tag{11}$$

Furthermore, (11) can be vectorized as

$$\boldsymbol{f}(\boldsymbol{p}_{a,k}) = \boldsymbol{0} \tag{12}$$

where

$$\boldsymbol{f} = [f_1, f_2, f_3]^T. \tag{13}$$

Under the least squares criterion, the kth APC can be estimated by

$$\hat{\boldsymbol{p}}_{a,k} = \arg \min_{\boldsymbol{p}_{a,k} \in \mathbb{R}^3} \|\boldsymbol{f}(\boldsymbol{p}_{a,k})\|_2 \tag{14}$$

where $\mathbb{R}^3$ denotes the 3-D real space.

Now that we have obtained the APC estimation model (14), any unconstrained optimization method can be applied to solve it. After that, the standard BP can be performed based on the estimated APC.

Compared with GABP, LABP achieves the important performance improvement from two aspects.

1) For memory requirement: We just use three pixels in LABP. This means that we need to store the back-projected values for only three pixels. Compared with GABP, in which the per-pulse back-projected values for all the pixels must be stored, the memory requirement is largely reduced. For example, if the APC number is also $K = 5000$, no matter how large the scene is, we need only $8 \times 3 \times K \approx 117$ kB $(M = 3)$ for the back-projected values in the autofocus procedure. This amount is much smaller than the memory requirement for GABP, which is 149 GB.

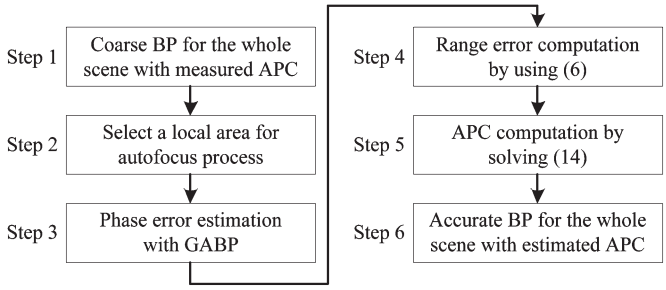

Fig. 2. LABP algorithm flow.

2) In terms of speed: On the one hand, the use of much less pixels greatly reduces the computation in the autofocus procedure. On the other hand, the separation of the subsystems from the large system can accelerate the convergence. Moreover, the iteration in GABP disenables the parallel processing, but the improved process releases the standard BP from the iteration clearly and the excellent parallel property of the standard BP makes it realizable on the graphics processing unit (GPU) [14]. This parallel processing will further accelerate the imaging by a large amount.

Note that the aforementioned derivation is theoretical more or less. In practical application, more problems should be considered.

First, because the problem of phase error wrapping is not considered in GABP, the phase $\hat{\phi}$ obtained through getting the phase of $e^{j\hat{\phi}}$ may be still wrapped if the range error is larger than λ, and then, the reversely calculated range error in (6) will deviate from the true range error by $L \times \lambda$, where L is the wrapping number. To avoid the phase wrapping, the allowed range error should be limited within λ. This limitation is too strict for the high-resolution imaging. However, if the IMU is used in the SAR system, the measured range error may be less than λ. Even if the measured range error is beyond λ, LABP can be still applicable. In this situation, whether for LABP or for GABP, although the estimation of the single phase correction value is not accurate for phase compensation, the cumulative result along the full synthetic aperture makes the sharpness-optimized phase error best for the focus of the image. Of course, when the range error is on the order of several meters, the performance of LABP decreases.

Second, it is best to select the strong scattering pixels to get higher performance. We can use the standard BP with linear APCs to get a coarse image and to find the strong points at first. However, this method may fail if there are no strong scatters in the scene. Another more efficient way to improve the performance is to choose a small region in the scene that should include most of the dispersed energy of the relatively strong pixel and to form an overdetermined system. This system can be also solved in the optimization method, and the memory requirement will not increase too much. For example, if the APC number is also $K = 5000$ and the size of the selected area is $M = 5 \times 5$, the required memory is only about $8 \times M \times K \approx 1$ MB. This is still quite small compared with GABP.

Considering the practical application, the LABP algorithm flow is sketched in Fig. 2. In step 1, if the IMU or other measurement sensors are used, the measured APC can be obtained

TABLE I
SIMULATION PARAMETERS

Quantity	Value	Quantity	Value
carrier frequency	10 GHz	platform mean altitude	4000 m
pulse width	1 μs	platform velocity	100 m/s
bandwidth	300 MHz	nearest slant range	5000 m
sampling rate	390 MHz	scene size	60 $\times$ 60 pixels
PRF	500 Hz	pixels interval	0.5 m $\times$ 0.5 m
synthetic time	0.6 s	APC number	300

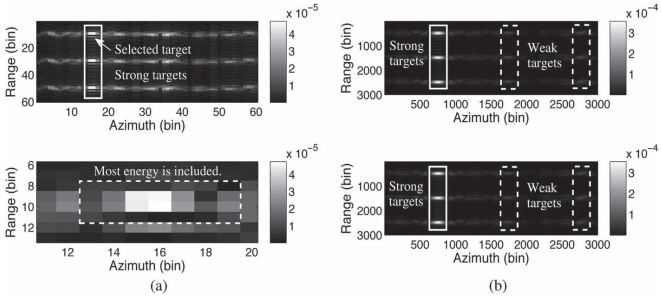

Fig. 3. Imaging results. (a) (Upper) Coarse image and (lower) selected region for LABP. (b) Resampled image with GABP (upper, time: 129.5 s, memory: 16.5 MB) and LABP (lower, time: 5.2 s, memory: 112.5 kB).

through measured data preprocessing. If there is no measurement sensor, the measured APC can be replaced with the linear trajectory. In step 2, in order to get higher APC precision, the selected local area should be larger. However, if this area is too large, the time consumption in step 3 will be very high; thus, it is best to make a tradeoff.

IV. EXPERIMENTAL RESULTS

In this section, both the point target simulation and the real data experiment are performed to verify the efficacy and efficiency of the LABP.

A. Simulation and Analysis

The parameters are listed in Table I. Simply but also in general for airborne side-looking SAR, we add the random uniform noises between -0.5 m and 0.5 m (much larger than λ) to the height of the platform to simulate the nonlinear trajectory, ignoring the instability in other directions. Five iterations are performed when estimating the phase error vector in both GABP and LABP.

The coarse image containing nine point targets by using the linear trajectory is illustrated in the upper subplot in Fig. 3(a), which is seriously defocused. A rectangular region (4×6 pixels) around the strong points is selected as the autofocus pixels in LABP. This region contains the most dispersed energy of the strong point. The imaging results with GABP and LABP are shown in Fig. 3(b). In both the two subplots, the strong points are all well focused, and the other points are not focused so well. It can be seen that, as well as LABP, GABP also aims to focus the strong points in principle; thus, the performance of LABP will not decrease too much compared with GABP, although the used information of the scene is much less. Without performance loss, the speed of LABP is improved

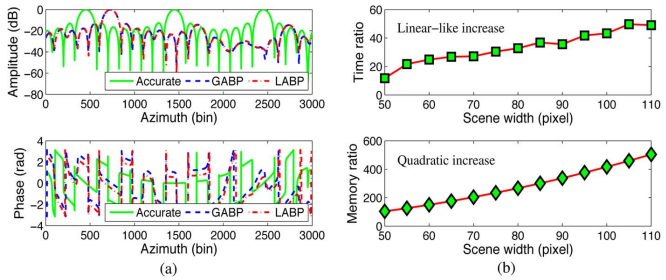

Fig. 4. Detail comparison. (a) Amplitude and phase of the middle-row azimuth profile in Fig. 3. (b) Time and memory ratio (GABP/LABP).

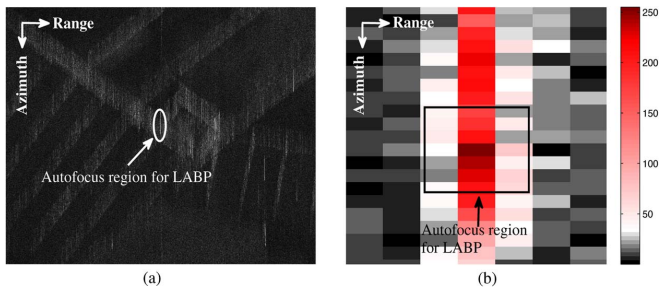

Fig. 5. Real data processing result with linear APC. (a) Whole scene. (b) Enlarged autofocus region for LABP.

by about 25 times, and LABP only requires about a hundredth of the memory occupied by GABP.

The amplitude and phase of the azimuth profiles in Fig. 3(b) are compared with the accurate image, and the result is shown in Fig. 4(a). For GABP and LABP, both the amplitude and the phase are close, and the point targets deviate away from their real positions. The reason for the latter is that the motion errors lead to the strong targets wrongly located in the coarse image, but GABP and LABP cannot correct the positions. However, the results confirm that LABP has nearly the same focusing performance as GABP.

Furthermore, the time ratio and the memory ratio of GABP to LABP in terms of the scene width are illustrated in Fig. 4(b). The time ratio linear likely increases with the scene width. The memory for both the back-projected values and the intermediate matrices is counted. We see that the memory ratio quadratically increases with the scene width. The feature of both the two curves further indicates the efficiency and memory advantages of LABP, and the advantages become more prominent with the increase of scene size.

B. Real Data Processing

In our airborne SAR data collection system (X-band, range resolution: 0.5 m, azimuth resolution: 1 m), there is no IMU to measure the antenna attitude errors. Therefore, we can only use the linear APCs based on the uniform linear motion model for imaging. The mean height and velocity of the platform are 5 km and 220 m/s, respectively. The scene size is 1000×1000 pixels with the interval of 1 m $\times$ 1 m. Five thousand APCs are used for imaging. The rough imaging result is shown in Fig. 5(a), which is seriously defocused in the azimuth direction.

When applying LABP, we select a small region around the strong point from Fig. 5(a) for autofocus, as shown in Fig. 5(b). We can see that this region includes 3×7 pixels with the most

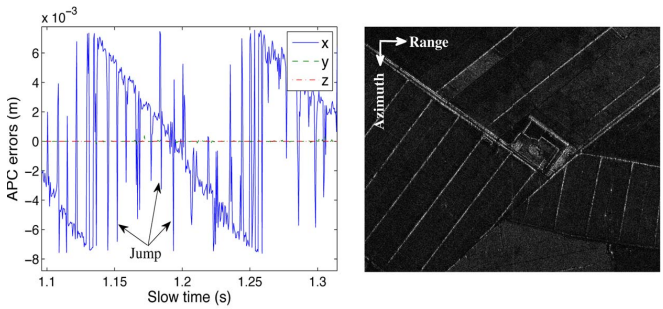

Fig. 6. Real data processing result with LABP. (a) Errors between estimated and linear APCs (partial plot). (b) Well-focused image.

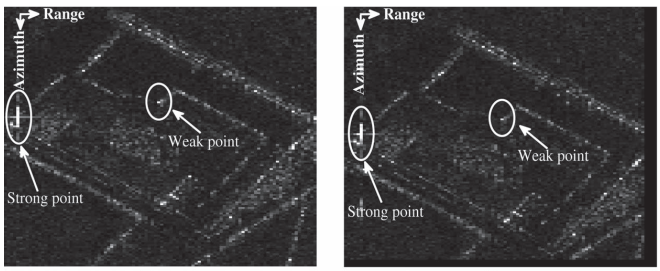

Fig. 7. Partial area imaging results. (a) GABP. (b) LABP.

dispersed energy of the strong point. The errors between the estimated APC and the linear APC are illustrated in Fig. 6(a). The three coordinate components are indicated by the blue solid line, green dashed line, and red chain line, respectively. It can be found that the deviations in both the azimuth and the height directions are very small. These deviations have little influence on focusing. However, the big vibration in the range direction is the main reason that leads to the defocus. Moreover, we can see many jumps at adjacent two slow times. This phenomenon reflects the wrapping of phase errors. The corrected imaging result is shown in Fig. 6(b). Obviously, the image is well focused, and the house and ridges can be clearly recognized.

On the other hand, GABP is incapable of processing the real data with a scene size of 1000 × 1000 since the required memory is too large to be satisfied on our computer. In order to compare the performance of LABP and GABP when processing the real data, a smaller scene with 140 × 100 pixels is selected from Fig. 5(a). The interval between pixels is 2 m × 2 m to include the house in the middle of Fig. 5(a) and the same strong point as used for Fig. 6(b). The number of APCs is reduced to 4000. The imaging results with GABP and LABP are shown in Fig. 7. We can only see that the image with LABP is shifted relative to Fig. 7(a). For detailed comparison, the azimuth profiles of the strong point and a weak point in Fig. 7 are illustrated in Fig. 8. Obviously, the azimuth focusing performance of LABP is almost identical to that of GABP.

V. Conclusion

In this letter, we demonstrate an improved autofocus BP algorithm. Compared to the GABP, although the range error tolerance is also limited within 1 or 2 m, the new method has

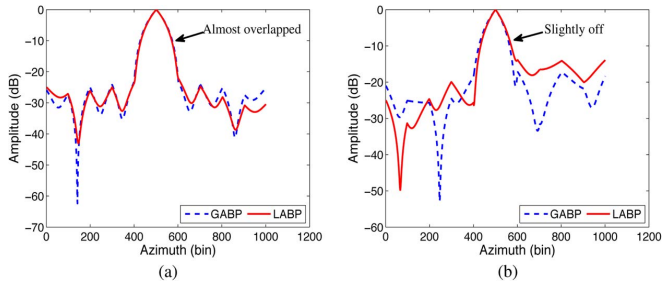

Fig. 8. Azimuth profile comparison. (a) Strong point. (b) Weak point.

two significant advantages: 1) The memory requirement is sharply reduced, and 2) the efficiency is improved by a large amount, particularly in the situation of large scene size. If the standard BP released from the iteration is transplanted onto the GPU, the process can be further greatly accelerated.

These two advantages are significant for the wide application of the autofocus BP algorithm, particularly in the real-time case or for small SAR systems.

References

[1] C. W. Sherwin, J. P. Ruina, and R. D. Rawcliffe, "Some early developments in synthetic aperture radar systems," *IRE Trans. Mil. Electron.*, vol. MIL-6, no. 2, pp. 111–115, Apr. 1962.

[2] Y. Ouyang, J. S. Chong, Y. R. Wu, and M. H. Zhu, "Simulation studies of internal waves in SAR images under different SAR and wind field conditions," *IEEE Trans. Geosci. Remote Sens.*, vol. 49, no. 5, pp. 1734–1743, May 2011.

[3] Z. G. Ding, L. S. Liu, T. Zeng, W. F. Yang, and T. Long, "Improved motion compensation approach for squint airborne SAR," *IEEE Trans. Geosci. Remote Sens.*, vol. 51, no. 8, pp. 4378–4387, Aug. 2013.

[4] G. Fornaro, G. Francechetti, and S. Perna, "Motion compensation errors: Effects on the accuracy of airborne SAR images," *IEEE Trans. Aerosp. Electron. Syst.*, vol. 41, no. 8, pp. 1338–1352, Oct. 2005.

[5] S. Ozsoy, "Pencil back-projection method for SAR imaging," *IEEE Trans. Image Process.*, vol. 18, no. 3, pp. 573–581, Mar. 2009.

[6] T. A. Kennedy, "Strapdown inertial measurement units for motion compensation for synthetic aperture radars," *IEEE Aerosp. Electron. Syst. Mag.*, vol. 3, no. 10, pp. 32–35, Oct. 1988.

[7] W. X. Tan, D. J. Li, and W. Hong, "Airborne spotlight SAR imaging with super high resolution based on back-projection and autofocus algorithm," in *Proc. IEEE IGARSS*, Boston, MA, USA, Jul. 2008, vol. 4, pp. IV-1300–IV-1303.

[8] D. E. Wahl, P. H. Eichel, D. C. Ghiglia, and C. V. Jakovatz, Jr., "Phase gradient autofocus-A robust tool for high resolution SAR phase correction," *IEEE Trans. Aerosp. Electron. Syst.*, vol. 30, no. 3, pp. 827–835, Jul. 1994.

[9] L. Zhang, H. L. Li, Z. J. Qiao, M. D. Xing, and Z. Bao, "Integrating autofocus techniques with fast factorized back-projection for high-resolution spotlight SAR imaging," *IEEE Geosci. Remote Sens. Lett.*, vol. 10, no. 6, pp. 1394–1398, Nov. 2013.

[10] T. M. Galloway and G. W. Donohoe, "Subaperture autofocus for synthetic aperture radar," *IEEE Trans. Aerosp. Electron. Syst.*, vol. 30, no. 2, pp. 617–621, Apr. 1994.

[11] M. Rodriguez-Cassola, P. Prats, G. Krieger, and A. Moreira, "Efficient time-domain image formation with precise topography accommodation for general bistatic SAR configurations," *IEEE Trans. Aerosp. Electron. Syst.*, vol. 47, no. 4, pp. 2949–2966, Oct. 2011.

[12] M. Liu, C. S. Li, and X. H. Shi, "A back-projection fast autofocus algorithm based on minimum entropy for SAR imaging," presented at the 3rd APSAR Conf., Seoul, Korea, Sep. 2011.

[13] J. N. Ash, "An autofocus method for backprojection imagery in synthetic aperture radar," *IEEE Geosci. Remote Sens. Lett.*, vol. 9, no. 1, pp. 104–108, Jan. 2012.

[14] J. Shi, L. Ma, and X. L. Zhang, "Streaming BP for non-linear motion compensation SAR imaging based on GPU," *IEEE J. Sel. Topics Appl. Earth Observ. Remote Sens.*, vol. 6, no. 4, pp. 2035–2050, Aug. 2013.